M.I.T Media Laboratory Perceptual Computing Section Technical Report No. 254

Temperature and Gibbs Image Modeling *

R. W. Picard and A. P. Pentland
MIT Media Laboratory; 20 Ames Street, Cambridge, MA 02139
Phone: (617) 253-0611, Fax: (617) 253-8874, Email: picard@media.mit.edu

Abstract: The Gibbs random field (GRF) has become a popular image model with applications in restoration, segmentation, reconstruction, edge detection, compression, and motion estimation. Its synthesis of natural-looking texture using only a small number of parameters is a key motivation for its widespread use. However, its wide use belies a number of difficulties inherent in the application of the model. In particular, it has proven difficult to control scale and patterning within the GRF framework, and to estimate parameters for a given pattern. The image processing literature has largely ignored the role of the temperature in the GRF, a parameter that appears in the original statistical mechanics formulation of the GRF. In applications such as simulated annealing, temperature is known to control scale, and in nature, temperature plays a critical role in multiresolution pattern formation, e.g., crystallization. Consequently, examination of GRF temperature parameters provides important insight into problems of scale and pattern formation. This paper presents (1) useful tools for characterizing temperature effects and points of "phase" transition, (2) characterization for the autobinomial GRF, (3) explanations of how temperature affects parameter estimation, segmentation region size, and various scale and pattern-forming behaviors of the model. The results allow more accurate and flexible control when the GRF is used as an image model.

1 Introduction

Gibbs random fields (GRF), and their equivalent Markov random fields, have recently been applied to image segmentation [1], [2], [3], [4], [5], [6], [7], edge detection [8], restoration [9], [10], [11], [12], [13], reconstruction [14], [15], coding [16] [17], and motion estimation [18]. Underlying these applications is the notion of representing an image as a random field of primarily local interactions, i.e., using the GRF as an image model.

However it has proven difficult to control scale and patterning within the GRF model. Meanwhile, alternate models that provide multiscale representations such as wavelets, pyramids, quadtrees, etc. have achieved noteworthy success. Although there are recent efforts [10], [6], [19], [20], to develop multiscale random fields or to combine them with another multiscale model, these methods assume a discrete number of scales. None facilitate continuous control over scale.

In nature, however, multiresolution pattern formation does not occur by discrete quadtrees or pyramids but by mechanisms such as variations in temperature. For instance, the process of annealing to obtain a regular crystal structure without defect requires extremely slow lowering of temperature. The intuition is that at high temperature the components of the crystal can move freely over large scale, whereas at low temperature the mobility is less and restricts changes to small scales. As the temperature changes, so does the scale.

These temperature effects are well studied in physical sciences such as crystallography, and have a counterpart in mathematical modeling and image processing via techniques such as simulated annealing. For instance, in the now classic paper of Kirkpatrick *et al.* [21], they state "the temperature distinguishes classes of rearrangements, so that rearrangements causing large changes in the objective function occur at high temperatures, while the small changes are deferred until low temperatures." The use of temperature to control scale is the key motivation behind the use of simulated annealing for solving large optimization problems.

Temperature also appears directly as a parameter, T, in the original statistical mechanics formulation of the GRF. Thus examination of GRF *temperature* provides a way to estimate and control *scale*, a critical problem in image processing and understanding.

1.1 The GRF as an image and texture Model: Importance of T

When applied to problems in image processing, it is typically assumed that the GRF is a prior for the original image which contains regions of various textures. The resulting posterior distribution is then maximized (maximum *a posteriori* or MAP solution). Although conceptually elegant, in practice, use of the GRF has encountered many problems.

For example, in the MAP framework when a GRF is used as a prior, $1/T$ controls the strength of the prior relative to the strength of the data. It has been observed that varying the range of $1/T$ over certain ranges has little effect on performance in some cases [1], [22], [23], [24], [25], [7], and drastic effect on stability of a solution in other cases [26], [14]. The potential applications of this framework are enormous in number. It is not the goal of this paper to present yet another MAP application, but rather to begin to clarify the confusion surrounding the choice of the $1/T$ parameter. In this paper we show how to characterize temperature ranges where fundamental changes in model behavior occur. We propose several helpful tools for characterizing these changes.

In texture synthesis, textures are drawn from samples of the GRF probability density function. The methods used to sample the GRF tend to involve decreasing a given energy function, and sometimes minimizing it. During the synthesis, a given set of fixed GRF parameters can produce many different patterns. This leads to confusion in relating a given set of parameters to a given texture. Since the range of parameters is directly related to the range of temperature, understanding the effects

*This work was supported in part by the National Science Foundation under Grant Nos. MIP 87-14969 and IRI-8719920, in part by the Defense Advanced Research Projects Agency (DARPA) monitored by the Office of Naval Research under Grant No. N00014-89-J-1489, and in part by the Rome Air Development Center (RADC) of the Air Force System Command and DARPA under contract No. F30602-89-C-0022.

of temperature is essential.

Synthesis examples will be shown in this paper for both isotropic and anisotropic homogeneous GRF's. The application of both cases to natural textures was studied by Cross and Jain [29]. Applications of GRF textures to more complicated natural scenes can be found in the list of references in the first paragraph of this paper. Although studying the application of the GRF to natural scenes is very important, the intentions of this paper are different. Here, the goal is more fundamental – understanding the role of temperature in image pattern formation.

In their overview paper on GRF's, Dubes and Jain [27] raise important questions to clarify the outstanding problems in Markov/Gibbs modeling. The first is "what regions of the parameter space lead to valid models?" and the second is "what regions in the parameter space put the process into phase transition?" In this paper we will argue that answers to these questions require a full understanding of the GRF temperature. Temperature effects have been carefully studied in the literature of physics and of optimization, but mostly ignored in image processing. Moreover, the importance (and difficulty!) of choosing and estimating GRF parameters has been noted in almost every field of application, but the close relationship between these problems and temperature has rarely been acknowledged.

Perhaps the foremost problem is understanding the effects of temperature parameters on pattern and scale, particularly at phase transitions (which are analogous to physical phase transitions such as freezing or boiling). This paper presents a characterization of temperature effects and a new method for analyzing significant points of transition for Gibbs texture modeling. This analysis allows us to provide some answers to the questions of Dubes and Jain and to more appropriately determine in which range of temperature to operate the GRF. These results ultimately allow more accurate and flexible control when modeling images with the GRF.

2 Background

2.1 GRF notation and assumptions

This paper focuses on the discrete Gibbs random field (GRF), defined as follows. Let an image be represented by a finite periodic $M \times N$ lattice $\mathcal{S}$ with neighborhood structure $\mathbf{N} = \{\mathcal{N}_s, s \in \mathcal{S}\}$ where $\mathcal{N}_s \subseteq \mathcal{S}$ is the set of sites that are neighbors of the site $s \in \mathcal{S}$. Every site has a gray-level value $x_s \in \Lambda = \{0, 1, \ldots, n-1\}$. Let $\mathbf{x}$ be the vector $(x_s, 1 \leq s \leq |\mathcal{S}|)$ of site gray-level values. A neighborhood structure is said to be *symmetric* if $\forall s, r \in \mathcal{S}$, $s \in \mathcal{N}_r$ if and only if $r \in \mathcal{N}_s$.

Given the symmetric neighborhood structure, one can define a Gibbs energy $E(\mathbf{x})$ on the lattice. A joint probability distribution is assigned to the Gibbs energy yielding the *Gibbs random field*,

$$P(\mathbf{x}) = \frac{1}{Z} \exp\left(-\frac{1}{T} E(\mathbf{x})\right), \tag{1}$$

where Z is a positive normalizing constant known in the physics literature as a *partition function* and T is the "temperature" of the field. There are many ways to define a Gibbs energy. The simplest and most popular for image region modeling is the Potts model,

Definition 1 *The energy for the homogeneous Potts GRF is*

$$E(\mathbf{x}) = -\sum_{s \in \mathcal{S}} \left(\sum_{r \in \mathcal{N}_s} \beta_r (2\delta_{x_s x_r} - 1) \right),$$

where the model parameters are given by β_r, and $\delta_{x_s x_r} = 1$ when $x_s = x_r$ and 0 otherwise.

Potts patterns resemble a high-level image segmentation (see Fig. 1). Typically, this model is combined with another one that models the texture *within* each region. The *autobinomial* Gibbs energy of [28], has been shown to synthesize a variety of natural looking image textures [29], [30].

Definition 2 *The energy for the homogeneous autobinomial GRF is*

$$E(\mathbf{x}) = -\sum_{s \in \mathcal{S}} \left(\alpha x_s + \sum_{r \in \mathcal{N}_s} \beta_r x_s x_r \right), \tag{2}$$

where the model parameters are α, the external field, *and β_r, the bonding parameters.*

In the case where $n = 2$, both the autobinomial and Potts model become the Ising model, a well-known model in statistical mechanics.

In studies of autobinomial GRF's as texture models,[31], [29], [30], the temperature parameter was absorbed into the bonding parameters. The latter have been assumed to be the parameters that characterize image texture.

2.2 Synthesis and annealing

GRF image data is typically synthesized iteratively, using a Monte Carlo method such as the Metropolis exchange algorithm [32]. In this algorithm a new state is formed by exchanging or "swapping" pairs of values in the current state. No new values can be created and none are removed, so the system is "closed" – its histogram remains constant. In this closed system it can be shown that the external field cancels [33], [30], leaving only the bonding parameters. The Metropolis exchange performs stochastic relaxation, which allows the energy to increase at a given step, as opposed to always decreasing it; this aims at preventing the pattern from getting "stuck" in a local minima.

In many applications the temperature parameter is lowered gradually during the Monte Carlo optimization or synthesis. This is called "annealing" after the physical process with the same name. The temperature is lowered and iterations continued until the pattern reaches its "ground state," defined by equilibrium at $T = 0$, or equivalently, the global minimum energy pattern. The number of iterations required to reach the ground state is usually astronomical; hence, there is a great need to identify ways to speed up the annealing process. One way to speed things up is to identify where the important regions of change are as a function of temperature, so that the temperature annealing can spend more time at these temperatures. The results of this paper show how to determine these regions. In this paper the Metropolis exchange was used for all the experiments. Experiments were conducted both with and without annealing; these cases will be clarified in the appropriate sections.

There is presently no known optimal choice for what schedule to use to decrease the temperature. The form used in this paper is that of the lower bound derived by Geman and Geman [9], the log form:

$$T_i = \frac{c}{\log(1 + \lfloor i / i_{eq} \rfloor)}, \tag{3}$$

where $i = 0, 1, \ldots$ is the iteration number, i_{eq} is the number of iterations it takes for the distribution to reach equilibrium at the current temperature, i.e., to approximate a sample of the Gibbs distribution at that temperature, and $\lfloor\ \rfloor$ indicates truncation. This form is commonly used in the literature with

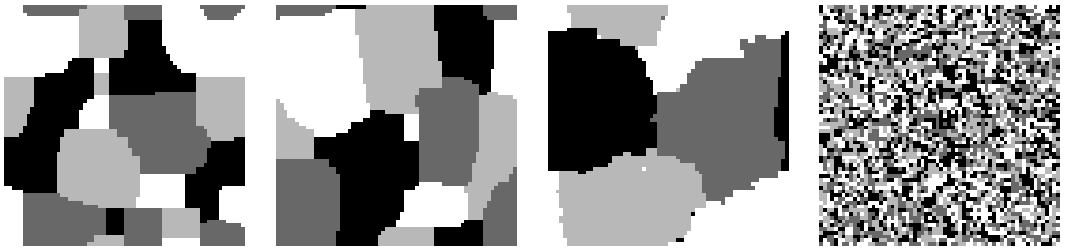

fastest $c = 1$, $T_{20,000} = 0.15$ | $c = 5$, $T_{20,000} = 0.72$ | $c = 10$, $T_{20,000} = 1.4$ | $c = 50$, $T_{20,000} = 7.2$ *slowest*

Figure 1: Potts GRF's synthesized with different annealing rates c. All images are 64×64 with $n = 4$ gray levels. All were synthesized for 20,000 iterations with the temperature lowered every 20 iterations according to the annealing schedule in (3).

the scale factor in the numerator typically chosen in the range $c \in (0, 10]$. Although its choice is ad hoc, its behavior is understood as a rate constant that is proportional to how slowly the annealing progresses.

Fig. 1 shows four GRF images made with different annealing rates using the Potts energy[1]. Notice in the progression of images for $c = 1, 5, 10$, that the pattern appears to be zooming in scale. At $c = 50$ the zooming no longer appears. There is some correspondence between temperature and scale as noted by many [35] [36], [22] [3]. But what is it? And for which region(s) in the model space? We have found that the temperature-scale correspondence is true only up to a critical point. In later sections we will demonstrate some ways to identify these points of critical changes.

In Fig. 1 the case with $c = 10$ has the least energy of the four cases – in other words, this particular choice of c resulted in the fastest progress to the minimum energy configuration, even though this was not the "fastest" rate. Here is an example where going slower (at $c = 10$ vs. $c = 1, 5$) saves time, where "slower" is controlled by temperature. What is the best range of temperature for a given model? Solutions can be found much faster if we first determine the best range of T to use.

The "best" range of temperature will of course depend on what is desired in the final image. For example, if the Potts model is used for image segmentation, and the leftmost sample in Fig. 1 best matches the desired region sizes, then synthesizing at $T = .15$ is best. To find a segmentation when the average region size is known in advance, choose a temperature that "prefers" that region size. Many have remarked that choosing the right temperature at various temporal or spatial positions can speed up and improve the solution in their application e.g., [36], [37], but none have shown how to go about finding these temperatures. We present some tools below for characterizing temperature, and apply them to autobinomial patterns. But the ideas behind the tools are general enough to be used for many other kinds of patterns.

2.2.1 Synthesis at constant temperature vs. annealing

As mentioned, a sample from the GRF, e.g., a texture, is synthesized iteratively by a stochastic relaxation method. Whether or not T is varied, i.e., whether or not there is simulated annealing, the iterations aim to lower the energy function $E(\mathbf{x})$. At a constant T, with an initially random configuration, the energy will typically start out high, and gradually lower with each iteration until some equilibrium is reached. The behavior is similar when annealing is used; in either case one can generate similar patterns. For example, running the Metropolis exchange at a constant value $T = 7.2$ for 20,000 iterations makes an image with a visually similar texture to that of Fig. 1 for the case $c = 50$. For high T equilibrium arrives soon; for such patterns it can be faster to sample at constant T than to use annealing. For low T, it can take forever to reach equilibrium. What constitutes "low T" or "high T" can be determined using the tools presented in the following sections.

2.3 Relation between Gibbs energy, co-occurrences, and A matrices

The significance of pairwise gray-level information for visual texture discrimination was advocated in 1962 by Bela Julesz [38]. Since then, co-occurrences, or equivalently, histograms of pairwise gray-level occurrences, have become a standard tool for processing images involving texture [39, 40]. In [41] it was shown that a class of Gibbs energy functions could be expressed in terms of "aura measures" which are closely related to co-occurrences.

This result will be useful for characterizing visual pattern changes caused by temperature. To proceed, we need to define a few terms. First, a neighborhood can be partitioned into K *subneighborhoods*, $\mathcal{N}_s^k$:

$$\mathcal{N}_s = \bigcup_{k=1}^{K} \mathcal{N}_s^k, \ \ \forall s \in \mathcal{S}, \tag{4}$$

where $\mathcal{N}_s^k \cap \mathcal{N}_s^l = \emptyset, \ \forall l \neq k$.

Also, the image sites can be partitioned into sets having the same gray level:

$$\mathcal{S}_g = \{s \in \mathcal{S} | x_s = g\}, \ \forall g \in \Lambda. \tag{5}$$

Now, an alternate form for the autobinomial Gibbs energy (without external field) can be obtained using the results of [42]:

$$E(\mathbf{x}) = - \sum_{g,g' \in \Lambda} g g' \sum_{k=1}^{K} \beta_k m^k(g, g') \tag{6}$$

where

$$m^k(g, g') = \sum_{s \in \mathcal{S}_g} |\mathcal{N}_s^k \cap \mathcal{S}_{g'}|$$

[1] It is an interesting phenomenon to notice in these images that only three gray levels come together at most vertices. This requires less energy than four gray levels coming together, and is very common in nature, e.g. the facets on a stick of chalk most frequently meet in 3's. It also shows up in a variety of GRF models applied to image segmentation, e.g., see the segmentations of [34].

is known as the "aura measure over $\mathcal{N}_s^k$." The "aura measure" satisfies the properties of a measure over a dilated region surrounding a pixel[2]. Here, the dilated region is $\mathcal{N}_s^k$, a subneighborhood of the Markov neighborhood. Intuitively, the aura measure indicates how much of each gray level is contained in that neighboring region.

From [42], we know that the aura measure over a set is equal to a sum of the co-occurrences taken over the displacements which can exist in that set. Hence, by relating the Gibbs energy to aura measures, it is related to co-occurrences.

The aura measure also has an interpretation as a "miscibility" measure. Thinking of gray levels as fluids, if $m(0,1)$ is large, then gray levels 0 and 1 are "mixed"; if small, they are "separated". This interpretation allows one to visualize types of patterns corresponding to high or low aura measures: if the measures $m(g,g'), g \neq g$ are low, then the gray levels tend to cluster. In Fig. 1, the measures $m(g,g'), g \neq g'$ are lowest for $c = 10$ and highest for $c = 50$.

By grouping the aura measures into an $n \times n$ matrix $\mathbf{A}$, and setting $\mathbf{g} = [0, 1, \ldots, n-1]^T$, the energy in (6) can be written as

$$E(\mathbf{x}) = -\sum_{k=1}^{K} \beta_k \mathbf{g}^T \mathbf{A}^k \mathbf{g}, \tag{7}$$

where $\mathbf{A}^k$ has as elements $m^k(g,g')$. Therefore, the anisotropic energy will be a linear sum of isotropic energy terms with weights equal to the bonding parameters. When the model is isotropic then $\beta_k = \beta$ and,

$$E(\mathbf{x}) = -\beta \mathbf{g}^T \mathbf{A} \mathbf{g}, \text{ where } \mathbf{A} = \sum_{k=1}^{K} \mathbf{A}^k. \tag{8}$$

Let $\mathbf{C}(d)$ be the co-occurrence matrix at displacement d. Then,

$$\mathbf{A} = \sum_{s+d \in \mathcal{N}_s} \mathbf{C}(d).$$

Using the above relationship, the energy is equivalent to the texture's auto-correlation formed over just the displacements occurring in the Markov neighborhood $\mathcal{N}_s$ [33]. Later, we will measure the effect of temperature T on the Gibbs energy, which by this relationship, will lead to a characterization of T relative to local correlation.

Notice that two textures with the same co-occurrences will have the same Gibbs energy (and textures with different co-occurrences may or may not have different energies.) Energy is the sole quantity measured during the texture synthesis, but examining energy alone will not discriminate textures as well as will examining the structure of the matrix $\mathbf{A}$, and hence of the co-occurrence matrices.

3 Some problematic behaviors of the GRF

There are a number of applications where a model is needed which is invertible, e.g. image coding, or where a model is needed which has a reasonably unique mapping between parameters and a given pattern, e.g. image recognition. It is also critical in these applications to answer questions such as "how stable" are the parameters – does a small perturbation in parameter space lead to a small change in the resulting pattern, and vice-versa?

[2]The aura measure is nonnegative, monotonic, and subadditive [42].

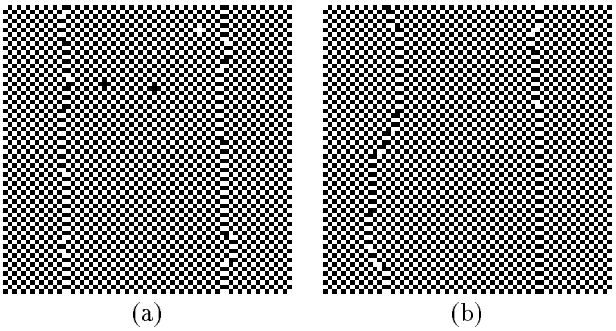

(a) (b)

Figure 2: Similar patterns made with different parameters. Pattern (a) has anisotropic parameters $\beta_1 = -1, \beta_2 = -2$. Pattern (b) was made with *isotropic* parameters, $\beta_1 = \beta_2 = -1$. The only other difference is the annealing rate: (a) $c = 2.7$ and (b) $c = 0.27$. Both images are binary, 64×64.

For texture modeling with the GRF, the bonding parameters, β_k, have been assumed by many in the literature to characterize a texture. In this section we illustrate that these parameters do not characterize a texture pattern in the way that has often been assumed. We also show that the texture may vary dramatically when a small change is made, such as increasing the number of gray levels in the random field. Later we will also show that over certain regions of parameter space, big changes in the parameters lead to small changes in the image (robust for image coding), while over certain other regions of parameter space, small changes in parameters lead to big changes in images (instability). The observations in this section are supported empirically; more formal analysis will follow.

3.1 Parameter non-uniqueness; image coding and recognition

As mentioned in the background, there is freedom in choosing energy functions; it is certainly possible to choose two different energy functions with the same minima, or to choose a single energy function with multiple minima. Since "ground state" refers to the global minimum energy configuration, it is no surprise that a given GRF can produce different looking patterns in its ground state. In the literature, it has also been the case that texture samples are drawn from a GRF at constant temperature that is not in equilibrium, even though it might look like things have stopped changing from iteration to iteration. In this case, even though the parameters are constant, numerous visually dissimilar patterns are produced as was illustrated in [43]. This poses a problem in texture synthesis of determining which pattern to associate with the parameters.

Fig. 2 shows an additional problematic example, this time where two visually similar patterns are made by dissimilar parameters. The isotropic $\mathbf{A}$ matrices differ by less than 0.1 % for the two patterns. Hence, two entirely different sets of parameters, one isotropic and one anisotropic, can generate the same type of pattern. In this case, recognition tests which looked at only the parameters might say these patterns are more different than they look.

An explanation of this latter non-uniqueness is easily obtained by considering the functions maximized for each set of parameters. Using the linear aura measure of (7), the energy minimized for (a) is

$$m^1(1,1) + 2m^2(1,1), \tag{9}$$

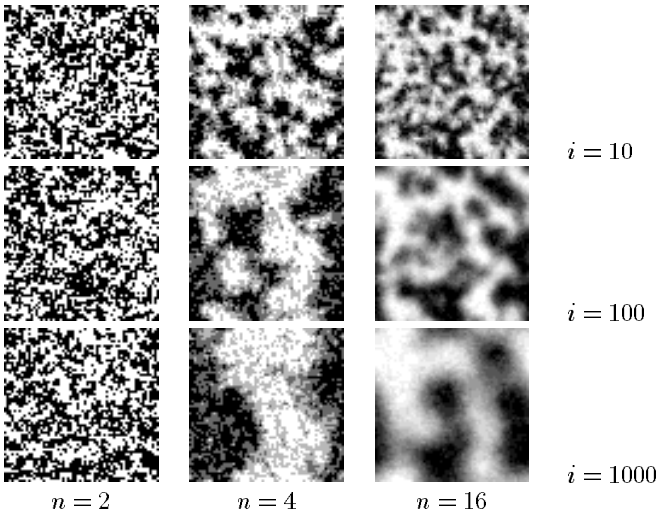

Figure 3: Number of gray levels effects pattern formation. The number of gray levels is $n = 2, 4, 16$ from left to right and the number of iterations is $i = 10$, 100, 1000, from top to bottom. Note there is more going on than a change in perceived resolution as you look from left to right. Meanwhile, looking down the columns, for $n = 2$ there is no change and for $n = 4, 16$ the pattern looks like it is being "zoomed" in scale. All twelve 64×64 textures have isotropic first order parameters $\beta = 1$.

and for (b) is:

$$m^1(1,1) + m^2(1,1). \tag{10}$$

A checkerboard pattern satisfys both $m^1(1,1) = m^2(1,1) = 0$ and the uniform histogram constraint. Hence the checkerboard configuration minimizes both (9) and (10), although neither pattern shown here has reached that minimum.

Nor is this a particularly special example; in the equilibrium GRF there is a condition of *positivity* which states that for all configurations, $\mathbf{x}$, the probability $P(\mathbf{x}) > 0$. Thus, unless we are in the ground state (equilibrium at $T = 0$), *all configurations are possible* even though some are more likely than others.

3.2 Sensitivity to number of gray levels

Many times it is desirable to work with a reduced number of gray levels. Fewer gray levels means fewer possible configurations, and less work for an optimization search. Ideally the number of gray levels, n, can be reduced without significantly destroying the percept of the texture – the resolution should only look a little worse. Similarly, increasing n should improve the resolution without changing the basic texture that is perceived. With the GRF, however, changing n, like changing T, can lead to very different behavior.

Consider the behavior when n is changed in the autobinomial GRF, as illustrated in Fig. 3. In Fig. 3, all the patterns have the same $T = 1$ and only the n is varied, left to right. For $i = 10$, one sees the desired effect from left to right, but for $i = 100, 1000$, the isotropic pattern does not merely look "smoother" with increasing n. For anisotropic textures the complexity of the behavior is even greater.

4 Temperature and application to parameter estimation

We have now seen several examples where texture pattern and scale are influenced by changes to the model parameters or changes in the number of gray levels. By including temperature in the model and studying its effects we will develop new explanations for the above phenomena which will help characterize and control texture formation for image modeling.

4.1 Model parameters as temperature annealing rates

In the temperature annealing schedule given in (3) the constant c is understood to be proportional to how slow the annealing progresses. From substituting the iteration-dependent temperature of (3) into (1) we obtain,

$$P(\mathbf{x}) = \frac{1}{Z} \exp\left(-\frac{\log(\lfloor \frac{i}{i_{eq}} \rfloor + 1)}{c} E(\mathbf{x}) \right), \tag{11}$$

or equivalently,

$$P(\mathbf{x}) = \frac{1}{Z} \left(\frac{1}{(\lfloor \frac{i}{i_{eq}} \rfloor + 1)^{1/c}} \right)^{E(\mathbf{x})} = \frac{B^{E(\mathbf{x})}}{Z},$$

where $B = \exp(-1/T)$ is the new base of the exponent. For a given energy, notice that changing the temperature is the same as merely changing the base of the exponent. As the number of iterations i increases, T decreases: $\lim_{i\to\infty} B = 0$. However, the larger the value of c, the slower the rate at which B goes to zero. Nature also exhibits a variety of behavior which can be attributed to a change of base in a power-law scaling model [44].

Dubes and Jain [27] pointed out that predicting pattern behavior from parameters is difficult; both the absolute and relative sizes of the parameters affect the pattern. We now derive results that help explain the behavior of patterns as a function of the *relative* sizes of the parameters. The importance of the *absolute* size of the parameters will be addressed subsequently. Both have direct impact on the modeling of images.

The formulation here is for the autobinomial model although a similar procedure can be followed for many other Gibbs models. Let $E^k(\mathbf{x}) = -\mathbf{g}^T \mathbf{A}^k \mathbf{g}$ be the portion of energy in the kth isotropic subneighborhood. Also, let temperature be a function of both iteration i and subneighborhood k. The bonding parameters, β_k can be grouped to scale the annealing rate, resulting in

$$T_{ik} = \frac{c/\beta_k}{\log(\lfloor \frac{i}{i_{eq}} \rfloor + 1)},$$

Substituting into (11) gives an alternate expression for the anisotropic GRF in terms of "anisotropic temperatures":

$$P(\mathbf{x}) = \frac{1}{Z} \prod_{k=1}^{K} \exp\left(-\frac{1}{T_{i,k}} E^k(\mathbf{x}) \right). \tag{12}$$

If Z could be factored, then (12) would become a product of independent fields. The analytic form for Z is not known in general, greatly complicating most work with GRF's. Except for Z however, each of the k directions acts like an isotropic field: each field has its own annealing rate constant, which controls its progress toward its ground state.

Let's revisit the analogy between fluids and gray levels, where patterns can be described by mixing and separation. The

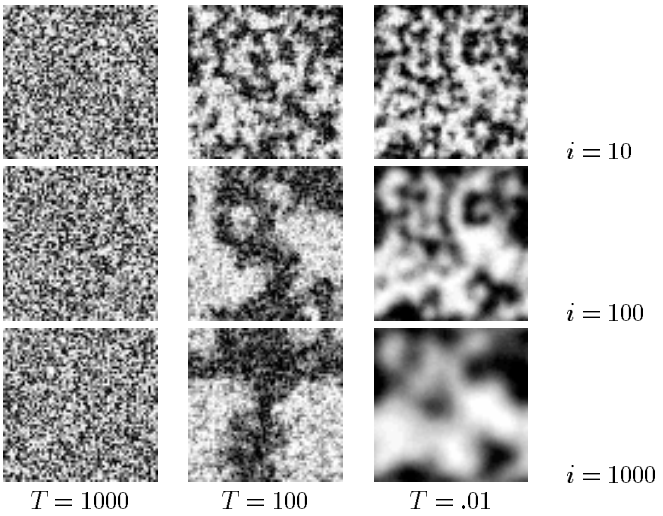

Figure 4: High temperature T impedes pattern formation and low temperature speeds it (over increasing iteration, i). All the samples are first order GRF's, 64×64, with $n = 32$ gray levels and isotropic $\beta = 1$.

rates can be thought of as controlling the progress of mixing or separation between gray levels in each direction. A person can watch the progress as the pattern is synthesized – or look at snapshots in time such as shown in Fig. 4.

Characterizing the "rates," i.e., finding changes to which they are proportional, is very difficult. The above manipulation shows that estimating the rates is like estimating the parameters. The latter is a notoriously difficult problem for this model.

4.1.1 Low and high temperature pattern formation

Consider Fig. 4 for an example of what happens if we synthesize using the same bonding parameters, but at several different temperatures. Since the parameters in this example are isotropic, synthesizing at different values T =1000, 100, .01 could be equivalently accomplished by setting $T = 1$ and synthesizing at $\beta/T = .001, .01, 100$. In the left column we see that the temperature is too hot for the pattern to form. Notice the similarity between Figs. 3 and 4. A decrease in temperature behaves like an increase in gray levels.

Several parameters might be of interest during GRF modeling, not just temperature. Nonetheless, studying the effects of temperature helps characterize the effects of changing the other values. Decreasing the temperature increases the absolute value of $\log(P(\mathbf{x}))$, the magnitude of the exponent of the random field, in a way that is similar to several other parameter changes – namely, increasing the magnitude of the bonding parameter, increasing the number of gray levels, and increasing the model order (i.e., the neighborhood size). Hence, these other parameter changes will influence the system in a way that can be characterized by temperature.

4.1.2 Equilibrium

Recall (3) where i_{eq} is the number of iterations required to allow the pattern to reach equilibrium. Equilibrium is a desired state for the GRF – when it is reached, then we can obtain a valid sample of the GRF density $P(\mathbf{x})$. In simulated annealing, this "equilibrium" implies that the energy levels off, i.e., the mean energy decrease is zero. A measure of the energy during synthesis of Figs. 3 and 4, shows that the energy is essentially constant for $n = 2$ and $T = 1000$, and decreases at various rates for the other cases (details are available in [33]).

Empirically the behavior we observed was always the same for higher n or for lower T: the GRF takes longer to reach equilibrium. Hence, if sampling textures with parameters that are large (corresponding to low values of T), then more iterations are needed; the same is true for images containing a large number of gray levels, n.

Using energy constancy as a measure of equilibrium, it is reasonable to conclude that in Fig. 3 equilibrium occurs in column $n = 2$ after 10 iterations, and in column $n = 4$ after 100 iterations. After about a thousand iterations the $n = 16$ energy decrease is also near zero, though not shown here. Even if the energy level is constant, the texture can still change in appearance; equilibrium does not imply the pattern has stopped changing.

4.1.3 Anisotropic interaction and equilibrium

Anisotropic patterns have a curious impact on equilibrium. According to (12) the anisotropic field cannot be completely decoupled into isotropic subfields unless Z is factorable, which is unknown (as is a closed form for Z). Consequently, this analysis is difficult and must be conducted empirically. Let's consider an anisotropic example, which gives some interesting behavior.

Example 3 *We wish to compare anisotropic behavior with its constituent isotropic behaviors. Suppose* $n = 32$ *as before, but now simulate* $T = 100$ *in the vertical direction and* $T = 0.01$ *in the horizontal. This can be achieved by setting* $T = 1$ *and* $\beta_1 = 100$, $\beta_2 = 0.01$. *We let the synthesis run 1000 iterations without annealing. The two images for the isotropic cases* $T = 0.01, 100$, *and image for the combined anisotropic* $\beta_1 = 100, \beta_2 = 0.01$ *are shown in Fig. 5. Features of its* $\mathbf{A}$ *matrix are discussed below.*

In Fig. 5 we see pattern clustering at low T on the left, a noisier pattern at high T in the center, and the result of combining these two effects on the right. However, instead of seeing the same amount of clustering as in the constituent directions, we see exaggerated horizontal clustering and vertical noisiness. The behavior is much more extreme than in the corresponding isotropic cases.

This "exaggerating" behavior can be captured quantitatively by features of the $\mathbf{A}$ matrix such as entropy [33]. If the entropy is computed for the isotropic $\mathbf{A}$ matrices of Fig. 5(a) and (b), and for the anisotropic $\mathbf{A}$ matrix of Fig. 5(c), then we find that the vertical anisotropic component has the highest entropy, the horizontal has the lowest, and the two isotropic components lie in between. Additionally, the sum of the two anisotropic components is close to the sum of the two isotropic components, suggesting that the average entropy is conserved.

With anisotropy, the horizontal direction (colder temperature, faster rate) takes advantage of the vertical direction (higher temperature, slower rate); the horizontal achieves lower entropy at the expense of the vertical – by moving faster, it "steals" correlation from the slower moving direction. This phenomenon manifests the non-separability of this model – the resulting effect is more exaggerated than its constituent isotropic effects.

Also, the horizontal anisotropic component changes more rapidly than the isotropic component at the same temperature. This behavior may imply that the anisotropic pattern is further from equilibrium. Other features of the $\mathbf{A}$ matrix [33] have also been studied, and shown to result in similar behavior.

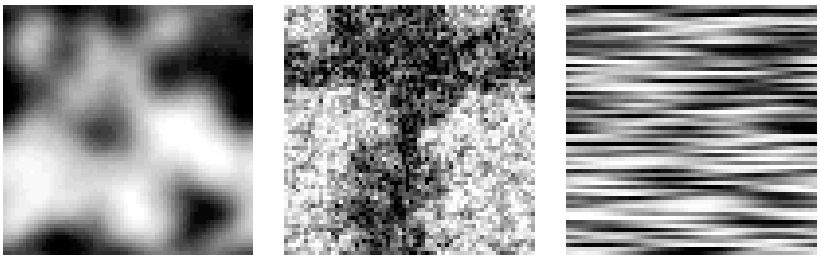

$T = .01$ $T = 100$ $T_h = .01, T_v = 100$

Figure 5: The first two patterns are isotropic and synthesized at constant cold $T = .01$ and hotter $T = 100$. The third is anisotropic, with bonding parameters set to simulate $T = .01$ in the horizontal direction and $T = 100$ in the vertical direction. All three are first order GRF's, 64×64, with $n = 32$ gray levels.

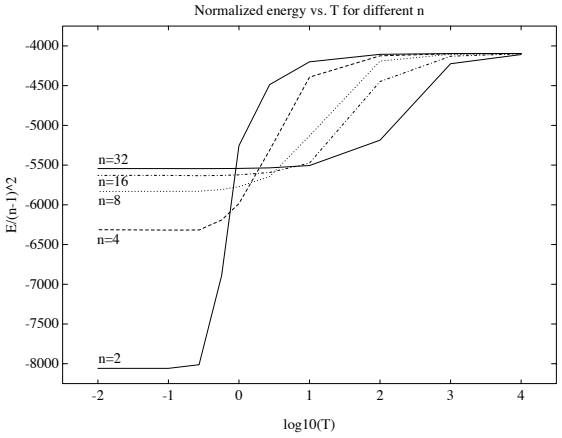

Figure 6: As the temperature decreases from right to left, energy drops. The normalized mean energy is shown for five different gray levels.

The ground states of all three textures in Fig. 5 can be shown to be identical, i.e., the same configuration minimizes both energy functions. If simulated annealing were used for their synthesis, eventually they would all look the same. It is here in their non-minimum energy states that their appearances vary so dramatically. To summarize, we have seen that bonding parameters can be interpreted as annealing rates, and patterns taken from *non minimum-energy* states exhibit exaggerated effects of interacting directional annealing rates.

4.2 Energy, temperature, and parameter estimation

Energy is what the synthesis algorithms measure; it depends on all the model parameters except temperature. When a pattern is in equilibrium at a given temperature then its average energy is constant. Energy is easy to measure, and its characterization is a common part of statistical mechanics. In this section we will explore energy as a function of temperature, and discuss its significance for the application of GRF image parameter estimation and for determining regions of desirable model behavior.

How does the mean energy change during long term synthesis of isotropic GRF's? Empirical results are shown in Fig. 6, where we allowed 10,000 iterations for the system to enter equilibrium (much more than necessary in most cases), and then computed the mean energy over the next 40,000 iterations.

Some details are in order. Energy grows with number of gray levels, n. Hence, the following normalization was made so that all the gray level cases can be easily compared. Assuming uniform histogram level, $|\mathcal{S}|/n$ and constant neighborhood size, $|\mathcal{N}| = \nu$, at high temperature the $\mathbf{A}$ matrix will be uniform. From the $\mathbf{A}$ matrix properties each row or column sum equals $|\mathcal{S}|\nu/n$. Thus, the energy at highest temperature can be expected to be

$$\mathbf{g}^T\mathbf{A}\mathbf{g} = \frac{|\mathcal{S}|\nu}{n^2}\sum_{i=1}^{n-1} i \sum_{i=1}^{n-1} i = \frac{|\mathcal{S}|\nu}{n^2}\frac{(n-1)n}{2}\frac{(n-1)n}{2} = \frac{|\mathcal{S}|\nu(n-1)^2}{4}.$$

In the results shown here, the mean energy was normalized by $(n-1)^2$ so that the high temperature values align for all gray levels. If lattices differ in the number of sites, $|\mathcal{S}|$, and neighborhood size, ν, then scaling by these is necessary to align the ranges. In Fig. 6 the normalized mean energy is plotted for $T \in \{0.01, 0.1, 0.27, 0.57, 1, 2.7, 10, 100, 1000, 10000\}$ and for $n \in \{2, 4, 8, 16, 32\}$. Most applications of GRF's have only operated on a few values of T, those near the middle of the large range shown here. Similarly, their bonding parameters have corresponded to the middle of this range.

We extended the temperature range much further than existing studies, to both hotter and colder temperatures until plateaus appeared in the energy vs. T plots at each end of the T axis. In addition to energy, we also measured four features of the $\mathbf{A}$ matrices, trace, entropy, correlation, and bandwidth, and found that all the features exhibited similar plateaus over the same temperatures. The empirical results held over simulations with several different "seeds" (for the Metropolis exchange). To our knowledge, this behavior has not previously been noticed in the image processing community, even though it has important implications for practical problems such as parameter estimation. The rest of this section focuses on applying these results.

4.2.1 Application to parameter estimation

These results provide a new way to estimate the temperature of a given texture, and an easy way to see why the estimation is hard. For a given image region (with some number of gray levels, n), one can compute the energy and use it to index into the energy vs. temperature curves of Fig. 6. Consider the energy for $n = 2$. The plot is monotonic around the values $T = 0.27$, 0.57, 1, 2.7, making temperature estimation straightforward in this region of "transition." However, for temperatures outside these values, the energy is constant. A similar behavior is visible for other values of gray level, n. Thus, we would expect

energy-based estimation to work well around the transition region, but not at the plateaus on each end.

For the isotropic GRF, the temperature estimation just described is equivalent to estimation of the GRF bonding parameters. Bonding parameter estimation is known to be difficult; it is nonlinear and the many methods that exist have been noted to have serious shortcomings. We discuss briefly a few of the problems, summarizing some of the ways the temperature results here can be applied.

Problem 1: uniqueness of the estimate. Assume there is a temperature T_r such that $T > T_r$ characterizes the right plateau. Since the energy and many other features of the $\mathbf{A}$ matrix are constant for all $T > T_r$, the variety of patterns that form there will be limited. If you measure the energy of a pattern and it maps to $T > T_r$, then there are an infinite number of parameters $T = 1/\beta$ to which it could correspond, e.g., there are cases where the same-looking data is synthesized with the parameter β and the parameter 100β. This "saturation" seems to have first been noted in the meterology literature by Garand *et al.* [30]. The plot of Fig. 6 shows a similar nonlinear pattern saturation occurs for low T. Saturation at high temperature is analogous to steam well above the boiling point; it doesn't change. A similar analogy holds at low T for ice. This concept is easily grasped with temperature, but is somewhat surprising for model parameters, $\beta = 1/T$.

Problem 2: equilibrium. Most of the patterns synthesized in the texture modeling literature do not appear to have been in equilibrium or in their minimum energy configurations. Hence, the parameters estimated for them will generally not correspond to the parameters used to synthesize them. Sometimes this may be the reason why a particular estimation method is "not working". To help prevent these problems, the tools and results discussed in this paper can be used to characterize equilibrium and to determine regions of valid parameter estimation.

Problem 3: insufficient training data. Most methods require all clique configurations to not only be represented in the samples presented for estimation, but to be represented in large number for accuracy in estimation. In comparing performance of estimation methods, Chen [45] noticed many autobinomial patterns did not contain enough of the different clique configurations to conduct estimation. This problem grows with the order of the cliques and with the number of gray levels; it is a case of the famous "curse of dimensionality."

The results above also indicate that the estimation problem gets worse at low temperature, where the energy tends to be near its minimum. For models such as the autobinomial GRF, minimum energy values are known [43] to correspond to zeros appearing in the $\mathbf{A}$ matrix, signifying the lack of existence of some clique configurations. Estimation algorithms that require all configurations to be present will thus fail below the temperatures where the zeros begin to appear in the $\mathbf{A}$ matrix.

An alternate route with estimation is to not count frequency of occurrence of clique configurations, but rather to consider the energy or the $\mathbf{A}$ matrix features. All of these are monotonic functions of temperature during the transition region. They can be used for recovering temperature even when all the configurations are not represented. The key limitation is that as long as the partition function is unknown for the general GRF, these regions must be determined empirically. This is a commonly accepted way to proceed in the natural sciences, but not in image processing, despite its easy implementation by look-up table.

Our results on temperature can be applied to some common problems with parameter estimation. For instance, Garand *et al.* [30], during Maximum Likelihood parameter estimation, reported that the parameter estimates were low when $n > 2$. They found they could fix the problem by scaling their Metropolis decision rule by a factor of 0.5. When this was done, their parameter estimates were closer to the parameters used for synthesis. This "ad hoc fix" has an appropriate explanation in terms of temperature. Pre-multiplication with their arbitrary scale factor is equivalent to setting $T = 0.5$, i.e., synthesizing at a lower temperature than the "no temperature default", $T = 1$. Decreasing the temperature has the same effect as increasing the parameter β, hence patterns are produced with higher effective parameter values.

It is insightful to also compare this estimation problem to the behavior pictured in Fig. 4. Allowing 100 iterations for equilibrium puts us in the second row of samples for the temperatures shown. When β/T is estimated for samples such as in Fig. 4, it will likely be accurate for the first two columns, but too low for the third column. When synthesis is stopped before equilibrium, the estimates tend to run low.

5 Phase transitions and application to texture modeling

Important changes in physical systems are characterized by their critical temperatures. This is well known in chemistry and physics, but has yet to be exploited in image modeling. Most people are familiar with the critical temperatures at which ice becomes water and water becomes steam, i.e., the points of *phase transition*. Very useful changes also occur in substances such as purified mercury where the critical temperature marks where the metal's resistivity goes to zero – it becomes superconducting.

For image processing, an important critical point is where a random pattern suddenly becomes structured. The chemical analogy is crystallization; the critical temperature is where the solution solidifies. The reconfiguring of a random arrangement of particles into a regular arrangement is a sought-after challenge for the random field texture model. Several people have suggested the importance of exploring phase transition phenomena for the GRF in image processing [2], [27], [46]. Phase transitions do not occur in a 1D GRF [47].

Technically, the critical points are the zeros of Z, the partition function. When Z is known, which it is for the Ising model and the Gauss Markov random fields (GMRF's), then the critical temperature(s) can be found analytically. For the Ising model there is one critical temperature, $T_c = 2.27$, which is the maximum value of T at which the center of the lattice is affected by the boundary conditions [47][3] Above T_c there is no long-range structure. For the GMRF, Z is the well-known normalizing factor involving the determinant of the covariance, and there is a critical point only if the covariance is singular. The valid GMRF parameter range can be found by imposing positive definite conditions on the Covariance matrix [49]. Lakshmanan and Derin [50] have recently found the valid parameter space for the GMRF on an infinite lattice. Valid parameters do not lead to singularities in Z; therefore, they do not yield phase transitions.

For the non-binary autobinomial GRF, Z is not known; therefore, its singularities and critical points must be found empirically. Strictly speaking, one dimension of the lattice needs

[3] This is obtained by letting $k_B = 1$ in the original formulation of Onsager [48].

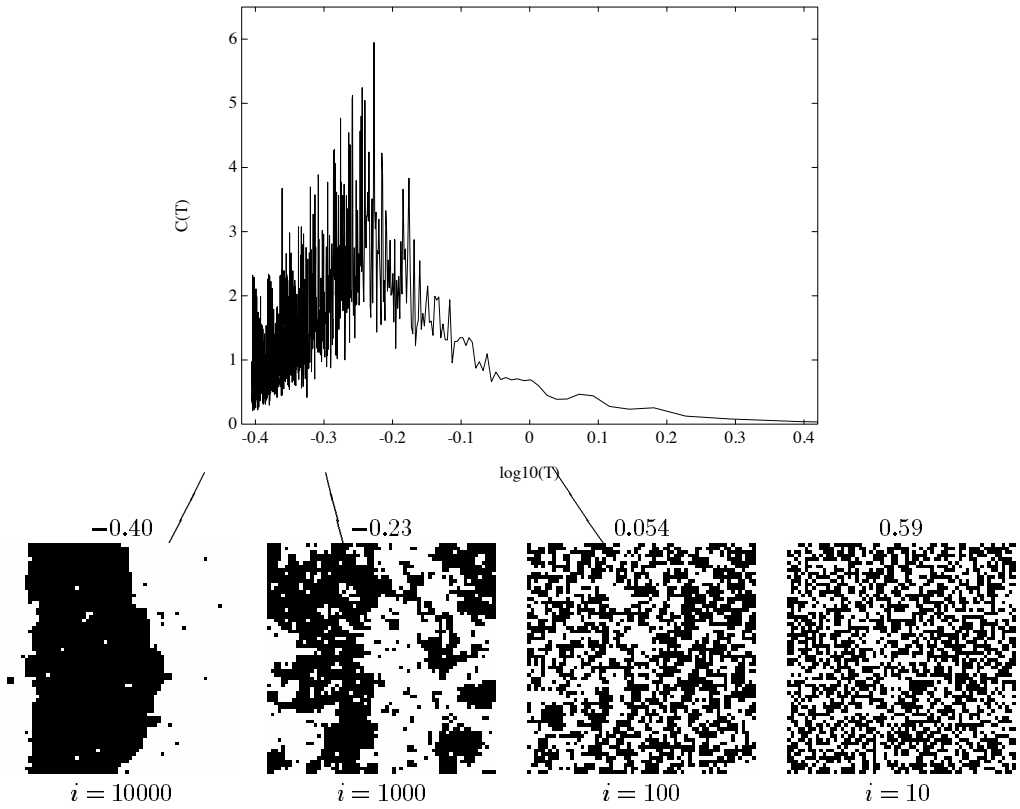

Figure 7: Ising model: Specific heat and patterns corresponding to above, near, and below critical temperature. Each image is 64×64, with $i_{eq} = 100$.

to go to infinity for a phase transition to exist. Thus, we can not find true "critical temperatures" for finite images. Even an approximate solution is difficult to simulate since the number of possible parameter combinations is infinite. Nonetheless, finite image data synthesized by a GRF can still exhibit abrupt changes in behavior that appear similar to phase transitions. We denote temperatures where the behavior changes significantly by T_*.

We discuss two methods for finding T_*, the first borrowed from the physics literature, the second newly proposed here. Both methods are implemented and illustrated below.

5.1 Specific heat to find T_*

In physics, the *specific heat* measures the change of energy with respect to temperature at a given volume or pressure. In simulated annealing this quantity has been approximated and found to have a large value when the state of order of the system was changing – as during phase transition. At a genuine critical temperature the specific heat would be infinite; however, for images, at T_* the peak of the specific heat is finite. We briefly review the formulation of specific heat for images, and show simulations running on a first order isotropic autobinomial GRF, with $\beta = 1$.

5.1.1 Formulation of specific heat

The specific heat is formulated as follows. In statistical mechanics the average energy is

$$< E(T) > = \frac{-d \ln Z}{d(1/k_B T)}.$$

The rate of change of the energy with respect to temperature gives the size of typical fluctuations in the energy at a given T [21],

$$\frac{d < E(T) >}{dT} = \frac{< E(T)^2 > - < E(T) >^2}{k_B T^2}.$$

This quantity is used in physics to approximate the specific heat. For texture measurements we normalize by the lattice size and omit the Boltzmann constant ($k_B = 1$), obtaining

$$C(T) = \frac{(< E(T)^2 > - < E(T) >^2)}{T^2 |\mathcal{S}|},$$

the specific heat for an GRF sample. The evaluation of the mean of the energy at T, $< E(T) >$, is the sum

$$< E(T) > = \frac{\sum_{i=1}^{i_{eq}} E_i(T)}{i_{eq}},$$

where $E_i(T)$ is the Gibbs energy at the current temperature and iteration, and i_{eq} is the number of iterations performed at each T during annealing.

Simulation: Ising model A simulation (see Fig 7) was first performed on the Ising model, to verify the method in a case for which the critical temperature is known (Onsager [48]) to be T_c such that $\sinh(2/T_c) = 1$. The variables in our implementation can be mapped to theirs, so that

$$T_* = \frac{T_c}{4} = 0.567,$$

which is close to the peak of the specific heat found at $T = 0.569$. Example patterns are shown below the plot of specific

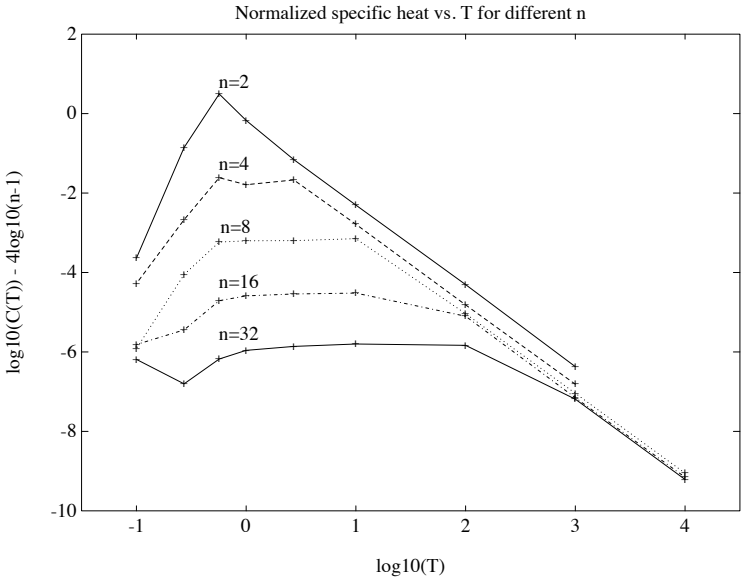

Figure 8: Specific heat (coarsely sampled) for five different numbers of gray levels, n. Peaks correspond to transition regions.

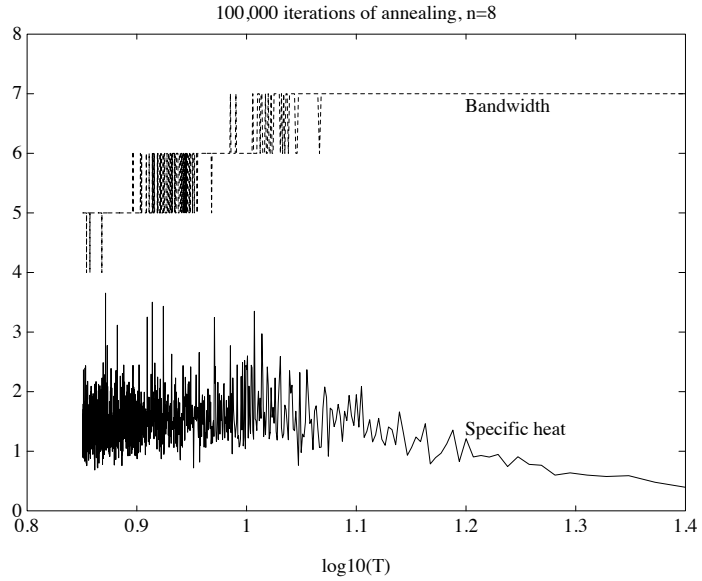

Figure 9: As the specific heat begins to increase, the bandwidth of the **A** matrix drops. This simulation is with $n = 8$ and $i_{eq} = 100$.

heat. A quick glance reveals that above T_* the pattern does not develop much, whereas below T_* separation of black and white occurs. One physical analogy is that the system is a gas at high temperature and a solid at low temperature.

In alternate applications, the peaked region has been found to be the place where freezing begins and where the process should be cooled most slowly to improve optimization [21] [51].

5.1.2 Problems: specific heat for non-binary images

The specific heat was successful in locating T_* for the binary case $n = 2$. However, three basic problems were found with using the specific heat when the image is not binary.

Problem 1: Peak depends on c. In simulations, the peak of the specific heat depends on c, the annealing rate. If c is not big enough, then the pattern will change extremely rapidly at the start of the process, causing a false peak. We determined empirically that if $c \geq (n-1)^2$ for a pattern of gray level n, then the specific heat will behave like the binary case – low at high temperature and peaked around T_c. It would be useful if a tighter lower bound could be placed on this value.

Problem 2: Peak too broad. The sharp peak in the binary case looses its sharpness as the number of gray levels is increased, making the beginning of the transition region hard to detect. Also, as can be seen in Fig. 9 the specific heat is very noisy.

Problem 3: Too long to reach equilibrium. Higher c implies a slower annealing rate and consequently, a longer time to reach equilibrium. A typical example is the bottom curve in Fig. 9 for an $n = 8$ texture. In this example after 100,000 iterations of annealing the specific heat has only been measured down to $T = 7.1$, midway in the transition region. To lower to $T = 0.5$ at this rate would take on the order of e^{98} iterations – absurd. The difficulty of doing a thorough characterization is immense.

To characterize behavior relative to temperature, it was necessary to find an alternative to the slow annealing. To do so, we sampled the temperature scale more coarsely, measuring specific heat at constant T for several values shown in Fig. 8. The values are normalized by $(n-1)^4$ and plotted on a log-log scale for closer comparison among different cases of n. Averages of the specific heat over 50,000 iterations and multiple seed values contribute to the final value shown at each point. (This is an excessive number of iterations for most cases, but was an effort to insure equilibrium measures.) The specific heats are shown in Fig. 8, normalized by $(n-1)^4$ and plotted on a log-log scale for closer comparison.

For all n, the specific heat is minimum at high temperature. For $n = 2, 4$ $\log_{10} C(T)$ is not shown because the energy variance is zero. For $n < 32$ the increase in $C(T)$ is linear from the minimum at the right to the first peak moving left, a case of "self-similarity" as found in fractal processes. On the far left $C(T)$ drops, except for $n = 16$ and $n = 32$. These two extreme points probably do not correspond to equilibrium conditions.

The results indicate that the specific heat method for finding T_* works fine for $n = 2$ but not for $n > 2$ since the peaks broaden with increasing n. The results also indicate that adding more gray levels raises T_*; this was recently verified by Elfadel [41] using a correlation approximation method in which the raise is by the factor $\frac{n^2-1}{3}$. The changing of the critical temperature by adding something to a solution is not new; a familiar example is the addition of salt to lower the freezing point of ice on slippery Winter streets.

In the next section we illustrate a different reason why the peak broadens with the number of gray levels – the presence of a new transition for each new gray level, and correspondingly new regions of distinct pattern behavior. The specific heat method fails to detect these separate transitions, but we introduce a new method which can detect them.

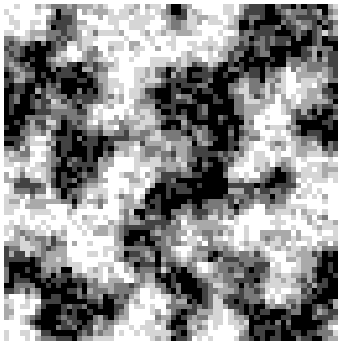

$$\mathbf{A} = \begin{bmatrix} 1454 & 859 & 345 & 60 & 10 & 0 \\ 859 & 908 & 685 & 229 & 42 & 5 \\ 345 & 685 & 848 & 596 & 201 & 53 \\ 60 & 229 & 596 & 870 & 632 & 341 \\ 10 & 42 & 201 & 632 & 974 & 869 \\ 0 & 5 & 53 & 341 & 869 & 1476 \end{bmatrix}$$

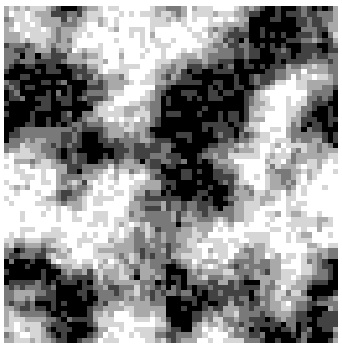

$$\mathbf{A} = \begin{bmatrix} 1714 & 839 & 160 & 15 & 0 & 0 \\ 839 & 1104 & 658 & 124 & 3 & 0 \\ 160 & 658 & 1128 & 661 & 116 & 5 \\ 15 & 124 & 661 & 1136 & 631 & 161 \\ 0 & 3 & 116 & 631 & 1104 & 874 \\ 0 & 0 & 5 & 161 & 874 & 1704 \end{bmatrix}$$

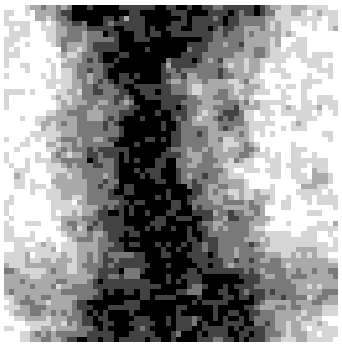

$$\mathbf{A} = \begin{bmatrix} 1868 & 822 & 37 & 1 & 0 & 0 \\ 822 & 1418 & 466 & 22 & 0 & 0 \\ 37 & 466 & 1550 & 649 & 25 & 1 \\ 1 & 22 & 649 & 1524 & 496 & 36 \\ 0 & 0 & 25 & 496 & 1440 & 767 \\ 0 & 0 & 1 & 36 & 767 & 1940 \end{bmatrix}$$

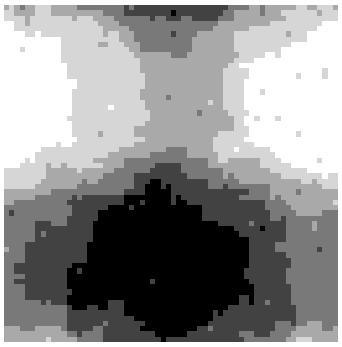

$$\mathbf{A} = \begin{bmatrix} 2546 & 182 & 0 & 0 & 0 & 0 \\ 182 & 2288 & 258 & 0 & 0 & 0 \\ 0 & 258 & 2248 & 222 & 0 & 0 \\ 0 & 0 & 222 & 2256 & 250 & 0 \\ 0 & 0 & 0 & 250 & 2292 & 186 \\ 0 & 0 & 0 & 0 & 186 & 2558 \end{bmatrix}$$

Figure 10: Patterns and their **A** matrices, undergoing bandwidth transitions. At the top the pattern has bandwidth four with $m(0,5) = 0$; hence no black and white pixels occur in the same neighborhood. The bottom image has minimum bandwidth for a six gray level image; hence neighboring pixels will not differ by more than one gray level.

5.2 Bandwidth transitions to find T_*

Many have studied critical phenomena for the Ising model [52], such as Pickard's study [53] using correlation. It has been shown [54] that co-occurrences give more discriminatory information than correlation for comparing image textures. The **A** matrix is built out of co-occurrences, so it can provide several second-order features in addition to correlation. These features do not appear to have been previously examined for critical phenomenon studies. In [33] four features of the normalized **A** matrix were studied during pattern formation: correlation, entropy, trace, and bandwidth. Of these, the bandwidth was found to be most useful for detecting temperatures that correspond to significant changes in autobinomial patterns when $n > 2$. Experiments below are for the same GRF parameters as in the previous section, to facilitate comparison between the specific heat method and the new bandwidth transition method.

Definition 4 *The* **bandwidth** *of a symmetric $n \times n$ matrix is the number of consecutive super-diagonals that have a non-zero entry. For a bandwidth of k, all elements (i, j) with $|i - j| > k$ must be zero.*

When $n = 2$ the bandwidth cannot be decreased, for if $m(0, 1) = 0$ then the two gray levels in the image would never be neighbors, and hence could not lie in the same image[4]. We found that for $n > 2$ the bandwidth changes throughout the regions where the specific heat was high. This suggests that the temperatures at the bandwidth discontinuities might also be "critical temperatures" [5]. The top curve in Fig. 9 shows the first three bandwidth transitions for the $n = 8$ example.

5.2.1 Precipitation in pattern formation

What do bandwidth drops correspond to in the visual pattern? Consider an example with six gray levels shown in Fig. 10. From top to bottom, the patterns undergo four drops in bandwidth. Each drop corresponds to a physical difference in the image, where pixels of one gray level cease to "mix" with pixels of another gray level. If each gray level is thought of as a different chemical substance, then at high temperature (random image, full bandwidth **A**) all the substances are "in solution". As the temperature is lowered, one by one the substances "precipitate" out of the solution.

If the image could physically break into separate images, at each precipitation point a different gray level would leave the image and form a new image of only that gray level. (An image with only one color minimizes the Gibbs energy.) The final minimum energy configuration would be n unicolor images.

For a texture of n gray levels, our empirical results indicate that there are $n - 1$ bandwidth drops, and thus n regions of temperature where a pattern can behave differently. These results allow use of temperature as a "control knob" for texture design, in much the same way as it is used chemically as a control for solubility.

Fig. 10 shows a first-order isotropic autobinomial GRF with $\beta = 1$. For isotropic fields with negative bonding parameters, the bandwidth decreases in the same way, but relative to the anti-diagonal. The theory for why the bandwidth becomes tridiagonal or anti-tridiagonal at minimum energy has been shown earlier [43]. Here the focus is on use of temperature to index into the pattern formation at non-minimum energy.

[4] It is possible to define a non-connected neighborhood and then obtain a diagonal **A** , but we adhere in this paper to the commonly used neighborhoods for GRF's. Hence, the minimum bandwidth is 2.

[5] To avoid new terminology, we will go ahead and use the terms "critical temperature" and "phase transition" even though, to be precise, they only apply to a finite lattice.

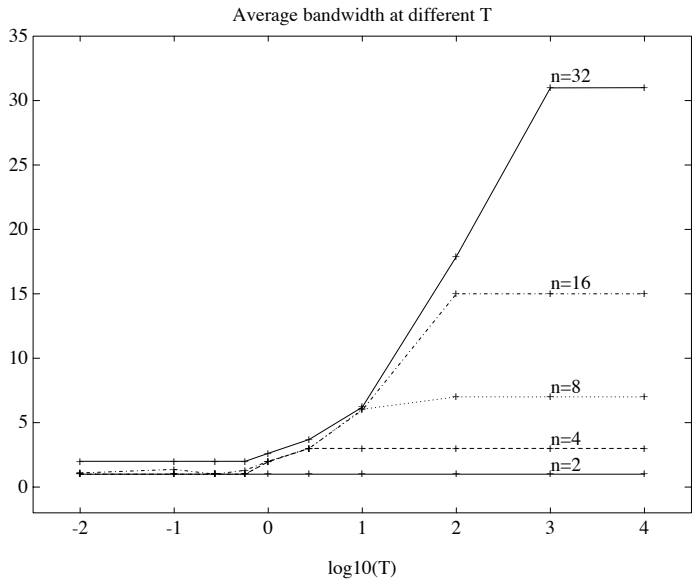

Figure 11: The bandwidths descend from n at high temperature to 1 at low temperature.

Relation to vector quantization The precipitation process also seems to be closely related in behavior to that described by Rose *et al.* [55] where the temperature is inversely related to the Lagrange multiplier in an optimization problem designed to find a vector quantizer. In that problem, as the temperature is lowered, the system passes through phase transitions which correspond to splitting of clusters. Here, the cluster-slitting is analogous to precipitation of the gray levels.

5.2.2 Empirical characterization: transition regions

We can see the patterning effects that correspond to different **A** bandwidth. How does bandwidth change as a function of temperature? We can answer this empirically with the results shown in Fig. 11 for $n = 2$, 4, 8, 16, 32. Each point was found by synthesizing at constant temperature and constant gray level for $i = 50{,}000$ iterations, more than necessary for most cases. Notice that cases $n = 2, 4, 8$ reach the minimum possible bandwidth, 1. Cases $n = 16$ and $n = 32$ have not yet attained this bound.

The individual regions are not sufficiently resolved in Fig. 11. Finer resolution can be obtained by combining temperature sampling and annealing. Results using log annealing with $c = (n-1)^2$, $i_{eq} = 100$, for 50,000 iterations and 64×64 samples are shown in Fig. 12. All the bandwidths are normalized by their maximum, $n - 1$ for comparison on the same plot.

Consider Fig. 12 for $n = 32$ gray levels. The unnormalized bandwidth drops from 31 to 20 over the temperature range $2.2 < \log 10(T) < 3.2$ in 11 visible levels. The downward trend is clear, although the bandwidth fluctuates along the way. As more time (relative to n) is spent at each temperature, sharper resolution is obtained. For $n = 16$ the 5 drops from bandwidth 15 down to 10 are sharper, and so forth.

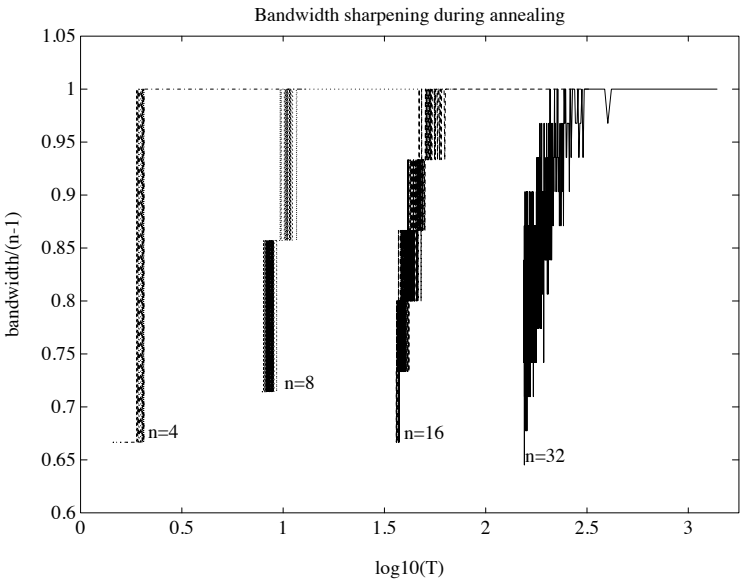

Figure 12: Bandwidths of aura matrices changing with temperature.

5.2.3 Specific heat vs. features of A

The two methods have their advantages and disadvantages. The specific heat method can be applied to any model. The bandwidth method is based upon some known results with the autobinomial model, although slightly different bandwidth results can be found for other models [43]. We mentioned that one problem with the method of specific heat for determining T_* is that the peaks of $C(T)$ change with the annealing rate, c. Similarly with the bandwidth method, it is important to choose c sufficiently large.

The bandwidth method has the advantage over the specific heat in that it associates distinct regions of behavior with distinct temperature regions. Thus it helps answer one of Dubes and Jain's questions, finding regions of temperature which put the process into transition. When the model is isotropic, these regions correspond directly to the parameter regions which cause transitions. The regions also correspond to perceptually distinct kinds of patterns – described as a sort of digital "precipitation."

5.3 Applications

Looking directly at aura measures (elements of **A**) instead of specific heat can also be used to characterize segmentation region sizes which occur at different temperatures. The diagonal terms of **A** give the amount of "mixing" of a color with itself; the off-diagonal terms give an approximation to the boundary length between regions. If the expected region size, or average edge boundary length between regions is known, then the known values can be compared to the aura measures during synthesis. For example, the traces of the **A** matrices for the Potts model examples of Fig. 1 monotonically increase from left to right with c, except for a sharp dip at $c = 50$. Hence, running the GRF while monitoring just the trace of the **A** matrix can find the desired size regions.

5.3.1 Convergence and equilibrium

Convergence criteria have been largely ad hoc in the image processing literature, and the question of equilibrium has been mostly ignored. Part of the reason for this stems from the lack of clear definitions of convergence and equilibrium, and part from a lack of understanding of temperature. If synthesizing a pattern in image coding or image reconstruction, the practical question is "when do you stop the iterations?"

For texture synthesis it is intuitively satisfying to stop the iterations and declare "convergence" when the pattern has "stopped changing." But this is a problematic definition for reasons involving both perception and measurement. In practice, "convergence" is usually defined as the meeting of some desired mathematical optimality criterion, the arrival at a global minima.

A state of "equilibrium" is similarly hard to define and to confirm. When annealing is done, the synthesis algorithm should be iterated i_{eq} times at the current temperature so that it will approximate an "equilibrium" sample of the Gibbs distribution at that temperature. In thermodynamics, a system is in equilibrium if no further changes occur in it when it is isolated [56]. At this point all its properties are homogeneous – there is no turbulence or pressure gradient, no diffusion, no reaction, no temperature gradient. The presence of any of these is the study of non-equilibrium states, often called "irreversible thermodynamics." Although non-equilibrium states are a rich source of texture patterns, it is difficult to characterize them with the current understanding of the GRF. In practice, we look to see when the energy stops changing, and declare this to be equilibrium.

Detecting equilibrium by measuring changes from iteration to iteration is tricky. In practice, the changes can be at such a slow scale, that even though they are proceeding relentlessly, the pattern will appear to have reached equilibrium. Fig. 3 shows such slow changes along the vertical axis – with rate of change more visible at higher n.

Since at an energy minima the energy stops changing, convergence to a minima implies equilibrium. Equilibrium can also imply convergence to the global minima if it occurs at $T = 0$. Also, it is a common trap to forget that even when the GRF is in equilibrium it will be constantly changing until it reaches its $T = 0$ equilibrium state. At $T \neq 0$, equilibrium does not imply convergence.

Convergence criteria in the literature The texture studies in the literature have stopped the synthesis process after ten to twenty iterations claiming "convergence" has occurred. These pioneering studies [31], [29], [30], defined convergence as either of the two following criteria being met:

- The number of pixels swapping in the Metropolis algorithm is sufficiently small;
- The estimated parameters of the synthetic texture are close to the desired parameters.

These definitions of "convergence" are not the same as the one described above. We now know that the amount of change in a pattern, and hence the percent of pixels swapping, depends on temperature and gray level. Hence, the first criteria is affected by temperature. Textures that are cooler have a smaller number of pixels swapping, and images with more gray levels (as with a lower temperature) have fewer pixels swapping at each iteration. Also, if a texture gets "stuck" in a local minimum, the number of pixels swapping will satisfy the first criterion even though the GRF has not converged to its maximum probability configuration.

The second criterion suffers from the problem that the bonding parameters do not uniquely correspond to a given texture sample. We illustrated this in Section 3, and showed in (12) that each parameter β_k controls the rate of mixing or separation in a particular direction.

For the autobinomial model, where the ground state configuration is known in terms of the **A** matrix, the bandwidth of the **A** matrix can be measured to monitor convergence. Using the results above, one can locate the temperature where the desired bandwidth lies, and speed up the synthesis process by iterating to equilibrium at that temperature. Furthermore, using connections recently established [42] between **A** matrix components and mathematical morphology, one can implement a computationally efficient algorithm for measuring the bandwidth.

5.3.2 Non-minimum energy texture synthesis

We have shown that qualitatively different textures correspond to temperatures above and below the temperature at the specific heat peak. Patterns which are far left of the peak correspond to minimum energy configurations. However, these patterns are not of interest in all applications; one may wish instead to synthesize non-minimum energy patterns. The results above provide tools to help control this synthesis.

For texture modeling, the above results bound the regions where the texture undergoes its abrupt bandwidth changes, and corresponding abrupt pattern changes. To synthesize a desired autobinomial pattern, one can measure its bandwidth structure and index into its most likely temperature region. Knowing the desired temperature range saves time by avoiding slow annealing in all the other regions. For the isotropic GRF, the temperature region dictates the valid parameter region. Hence, noting the locations of these "phases" is important before performing parameter estimation, helping avoid problems such as in Section 4.2.1.

Finding the critical temperatures for a given GRF is important for locating where long range structure can appear, i.e., below the critical point. In MAP applications, one typically wants to stay above this point, so that shortcomings of the prior are not introduced. Although the results reported here are for the case of zero or constant external field, the tools presented here are quite general, and can be used to investigate a wide variety of related GRF problems.

Periodic patterns with temperature variations Although the focus of this paper is on temperature, and not on texture synthesis or other applications of GRF's, a few synthesis examples do help illustrate the role of temperature. For example, suppose one wanted to synthesize a periodic texture. The obvious way would be to tesselate the plane with the texture primitives. In practice this gives a texture that looks too perfect to be natural. Nonlinear warping can help modify the periodicity, but it is a costly alternative and does not mitigate the artificial boundaries imposed by the tesselation.

Using temperature with the GRF gives an elegant solution to both these problems. Since the GRF is formulated on a periodic lattice there are no artificial boundaries induced by tesselating with Gibbs samples. With annealing or other temperature scaling, the samples can be taken at slightly different temperatures, or sometimes even at the same temperature, so that they are not perfect replicas of each other. Note that sampling at different temperatures can give a greater variety of effects than just taking different stochastic samples of the same state.

Fig. 13 shows two textures formed by replicating Gibbs samples with annealing and temperature scaling. The effect is more natural than perfect replication of a texture primitive. In addition the texture patterning can be controlled to duplicate many interesting effects. For instance, by introducing a temperature gradient from top to bottom (as was done in the right-hand image of Fig. 13) one can produce a perspective type of scaling. In other words, one can vary scale smoothly, with the "temperature control knob".

Note that although the examples in Fig. 13 are synthesized with replication, it is possible to have the random field produce the periodicity by partitioning it into independent regions prior to running the Monte Carlo synthesis. Each region is then its own "closed" system synthesizing its own random field. One could also construct hierarchies of such closed systems, building up increasingly complex textures.

6 Conclusions

The effect of temperature, T, in the GRF has been characterized and applied to problems in image and texture modeling. We have shown that:

1. There exists a transition region and outer plateau regions in the autobinomial energy as a function of temperature, T. In the transition region, T can be used to smoothly control changes in properties such as pattern scale.
2. For GRF models such as the Potts and autobinomial, temperature scaling varies the size of the regions most likely to occur in equilibrium. This has applications in image segmentation and region modeling. The Gibbs energy and/or the proposed **A** matrix features can be found as a function of temperature, and used to control these tradeoffs.
3. Above or below the transition region, the parameters can be changed by orders of magnitude and still correspond to visually similar patterns. This has applications to parameter estimation.
4. The GRF energy is not unique; hence, the GRF can not be applied to recognition, classification, or coding with the expectation that the model parameters correspond uniquely to the appearance of the synthesized pattern.
5. Within the transition region, the model parameters act as rates which affect the patterning. Certain choices of temperature and model parameters can speed synthesis when the desired pattern properties are known.
6. For anisotropic patterns, pattern formation in the direction of the faster rate can "steal" from the direction of the slower rate, causing quicker formation than would occur in an isotropic pattern forming at either of the constituent rates.
7. The method of specific heat is an effective tool for characterizing critical temperature in the binary model, but gives too broad of peaks for the general gray-level cases.
8. A new tool was demonstrated for finding temperatures of phase transition by looking at the bandwidth of the **A** matrix. This finds $n-1$ critical temperatures for a texture with n gray levels.
9. The regions between critical temperatures correspond to non-minimum energy patterns with a certain amount of "mixing" between gray levels. Temperature can be adjusted to give patterning with a desired mixing behavior.
10. Temperature can be used as a "control knob" to give variety to patterns for more natural replication, scaling, and perspective effects.

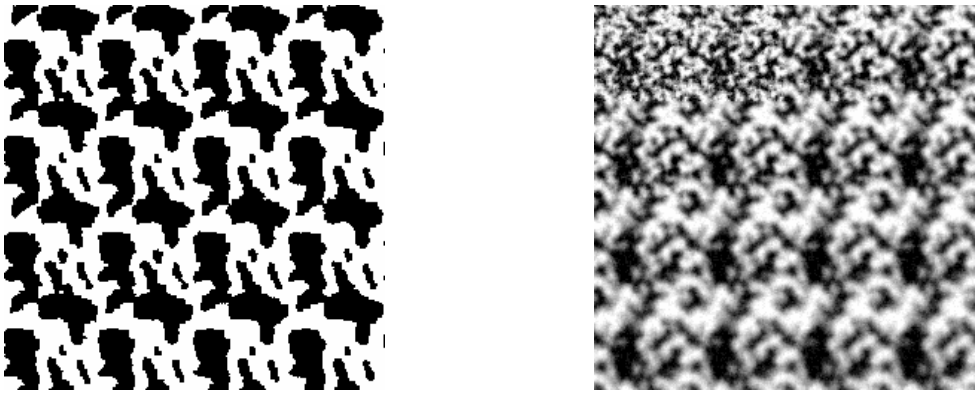

Figure 13: The use of temperature to create a "natural-looking", i.e., not perfectly periodic texture. Both patterns were made by replicating a 4×4 array of 64×64 samples of Gibbs distributions.

References

[1] H. Elliott, H. Derin, R. Cristi, and D. Geman, "Application of the Gibbs distribution to image segmentation," in *Proc. ICASSP*, (San Diego, CA), pp. 32.5.1–32.5.4, 1984.

[2] W. M. Lawton and M. Lee, "Random field models for use in scene segmentation," tech. rep., Jet Propulsion Laboratory, March 1985.

[3] H. Derin and H. Elliott, "Modeling and segmentation of noisy and textured images using Gibbs random fields," *IEEE T. Patt. Analy. and Mach. Intell.*, vol. PAMI-9, no. 1, pp. 39–55, 1987.

[4] S. Lakshmanan and H. Derin, "Simultaneous parameter estimation and segmentation of Gibbs random fields using simulated annealing," *IEEE T. Patt. Analy. and Mach. Intell.*, vol. PAMI-11, no. 8, pp. 799–813, 1989.

[5] J. K. Goutsias and J. M. Mendel, "Simultaneous optimal segmentation and model estimation of nonstationary noisy images," *IEEE T. Patt. Analy. and Mach. Intell.*, vol. II, pp. 990–998, Sept. 1989.

[6] C. Bouman and B. Liu, "Multiple resolution segmentation of textured images," *IEEE T. Patt. Analy. and Mach. Intell.*, vol. PAMI-13, no. 2, pp. 99–113, 1991.

[7] E. Rignot and R. Chellappa, "Segmentation of polarimetric synthetic aperture radar data," *IEEE T. Image Proc.*, vol. 1, pp. 281–300, Jul. 1992.

[8] D. Geman, S. Geman, C. Graffigne, and P. Dong, "Boundary detection by constrained optimization," *IEEE T. Patt. Analy. and Mach. Intell.*, vol. PAMI-12, no. 7, pp. 609–628, 1990.

[9] S. Geman and D. Geman, "Stochastic relaxation, Gibbs distributions, and the Bayesian restoration of images," *IEEE T. Patt. Analy. and Mach. Intell.*, vol. PAMI-6, no. 6, pp. 721–741, 1984.

[10] B. Gidas, "A renormalization group approach to image processing problems," *IEEE T. Patt. Analy. and Mach. Intell.*, vol. PAMI-11, no. 2, pp. 164–180, 1989.

[11] F.-C. Jeng and J. W. Woods, "Compound Gauss-Markov random fields for estimation," *IEEE T. Acoust., Sp., and Sig, Proc.*, pp. 683–697, March 1991.

[12] D. Geman and G. Reynolds, "Constrained restoration and the recovery of discontinuities," *IEEE T. Patt. Analy. and Mach. Intell.*, vol. PAMI-14, pp. 367–390, March 1992.

[13] J. Zhang, "The mean field theory in em procedures for blind Markov random field image restoration," *IEEE T. Image Proc.*, vol. IP-2, no. 1, pp. 27–40, 1993.

[14] D. S. Lalush and B. M. W. Tsui, "Simulation evaluation of Gibbs prior distributions for use in maximum a *posteriori* SPECT reconstructions," *IEEE T. Med. Imag.*, vol. MI-11, pp. 267–275, June 1992.

[15] C. Bouman and K. Sauer, "A generalized Gaussian image model for edge-preserving Map estimation," *IEEE T. Image Proc.*, vol. TIP-2, pp. 296–310, July 1993.

[16] T. R. Reed, V. R. Algazi, and I. Hussain, "Segmentation-based still-image coding in a perceptually transparent framework," in *Soc. for Info. Disp. Int. Symp. Dig.*, (Boston, MA), pp. 673–676, May 1992.

[17] R. W. Picard, "Random field texture coding," in *Soc. for Info. Disp. Int. Symp. Dig.*, (Boston, MA), pp. 685–688, May 1992.

[18] J. Konrad and E. Dubois, "Bayesian estimation of motion vector fields," *IEEE T. Patt. Analy. and Mach. Intell.*, vol. PAMI-14, pp. 910–927, Sept. 1992.

[19] F. Marques, J. Cunillera, and A. Gasull, "Hierarchical segmentation using compound Gauss-Markov fields," in *Proc. ICASSP*, (San Francisco), pp. III–53–III–56, 1992.

[20] S. Lakshmanan and H. Derin, "Gaussian Markov fields at multiple resolutions," in *Markov Random Fields* (R. Chellappa and A. Jain, eds.), Academic Press, 1993.

[21] S. Kirkpatrick, C. D. Gelatt, Jr., and M. P. Vecchi, "Optimization by simulated annealing," *Science*, vol. 220, no. 4598, pp. 671–680, 1983.

[22] J. Besag, "On the statistical analysis of dirty pictures," *J. Royal Stat. Soc., Ser. B*, vol. 48, pp. 259–302, 1986.

[23] F. Cohen and D. Cooper, "Simple parallel hierarchical and relaxation algorithms for segmenting noncausal Markovian random fields," *IEEE T. Patt. Analy. and Mach. Intell.*, vol. PAMI-9, pp. 195–219, Mar. 1987.

[24] B. S. Manjunath, T. Simchony, and R. Chellappa, "Stochastic and deterministic networks for texture segmentation," *IEEE T. Acoust., Sp., and Sig, Proc.*, vol. 38, pp. 1039–1049, June 1990.

[25] G. K. Gregoriou and O. J. Tretiak, "Unsupervised textured image segmentation," in *Proc. ICASSP*, (San Francisco), pp. III–73–III–76, 1992.

[26] D. Geman, "Random fields and inverse problems in imaging," Univ. of Mass. preprint, Dept. of Math. and Stat., 1989.

[27] R. C. Dubes and A. K. Jain, "Random field models in image analysis," *J. of Appl. Stat.*, vol. 16, no. 2, pp. 131–163, 1989.

[28] J. Besag, "Spatial interaction and the statistical analysis of lattice systems (with discussion)," *J. Roy. Stat. Soc., Ser. B*, vol. 36, pp. 192–236, 1974.

[29] G. R. Cross and A. K. Jain, "Markov random field texture models," *IEEE T. Patt. Analy. and Mach. Intell.*, vol. PAMI-5, no. 1, pp. 25–39, 1983.

[30] L. Garand and J. A. Weinman, "A structural-stochastic model for the analysis and synthesis of cloud images," *J. of Climate and Appl. Meteorology*, vol. 25, pp. 1052–1068, 1986.

[31] G. R. Cross, *Markov Random Field Texture Models*. PhD thesis, Michigan State Univ., 1980.

[32] N. Metropolis, A. Rosenbluth, M. Rosenbluth, A. Teller, and E. Teller, "Equation of state calculations by fast computing machines," *J. of Chemical Physics*, vol. 21, no. 6, pp. 1087–1092, 1953.

[33] R. W. Picard, *Texture Modeling: Temperature Effects on Markov/Gibbs Random Fields*. ScD thesis, M.I.T., 1991.

[34] A. Rangarajan, R. Chellappa, and B. S. Manjunath, "Markov random fields and neural networks with applications to early vision problems," in *Artificial Neural Networks and Statistical Pattern Recognition* (I. K. Sethi and A. K. Jain, eds.), pp. 155–174, Elsevier Science Pub., B. V., 1991.

[35] P. A. Flinn, "Monte Carlo calculation of phase separation in a two-dimensional Ising system," *J. of Stat. Phys.*, vol. 10, no. 1, pp. 89–97, 1974.

[36] J. L. Marroquin, *Probabilistic Solution of Inverse Problems*. PhD thesis, M.I.T., 1985.

[37] M. J. Black and P. Anadan, "Robust dynamic motion estimation over time," in *Proc. IEEE Conf. On Computer Vision and Pattern Recognition*, (Maui, HI), pp. 296–302, June 1991.

[38] B. Julesz, "Visual pattern discrimination," *Proc. IRE*, vol. 8, no. 2, pp. 84–92, 1962.

[39] R. Haralick, "Statistical and structural approaches to texture," *Proc. IEEE*, vol. 67, pp. 786–804, May 1979.

[40] L. Van Gool, P. Dewaele, and A. Oosterlinck, "Texture analysis anno 1983," *Computer Vision, Graphics, and Image Processing*, vol. 29, pp. 336–357, 1985.

[41] I. M. Elfadel, *From random fields to networks*. PhD thesis, M.I.T., 1993.

[42] I. M. Elfadel and R. W. Picard, "Gibbs random fields, cooccurrences and texture modeling," *IEEE T. Patt. Analy. and Mach. Intell.*, vol. 16, pp. 24–37, Jan. 1994.

[43] R. W. Picard and I. M. Elfadel, "Structure of aura and co-occurrence matrices for the Gibbs texture model," *J. of Mathematical Imaging and Vision*, vol. 2, pp. 5–25, 1992.

[44] M. R. Schroeder, *Fractals, Chaos, Power Laws*. New York: W. H. Freeman and Co., 1991.

[45] C.-C. Chen, "A nonparametric test for comparing estimators in Markov random fields," *Patt. Rec. Lttrs*, pp. 765–770, Nov. 1990.

[46] A. E. Smith, M. Gormish, and M. Bolick, "Physics and image data compression," in *Proc. SPIE Conf. on Image Proc. Alg. and Tech. III.*, vol. 1657, pp. 153–158, 1992.

[47] R. Kindermann and J. L. Snell, *Markov Random Fields and their Applications*. Providence, Rhode Island: American Mathematical Society, 1980.

[48] L. Onsager, "Crystal statistics I. A two-dimensional model with an order-disorder transition," *Physical Review*, vol. 65, pp. 117–149, 1944.

[49] N. Balram and J. Moura, "Noncausal Gauss Markov random fields: Parameter structure and estimation," *IEEE T. Info. Theory*, vol. 39, Jul. 1993.

[50] S. Lakshmanan and H. Derin, "Valid parameter space for 2-D Gaussian Markov random fields," *IEEE T. Info. Theory*, vol. 39, pp. 703–709, March 1993.

[51] D. E. Van Den Bout and T. K. Miller, III, "Graph partitioning using annealed neural networks," *IEEE T. Neural Networks*, vol. 1, no. 2, pp. 192–203, 1990.

[52] R. J. Baxter, *Exactly Solved Models In Statistical Mechanics*. London: Academic Press, Inc., 1982.

[53] D. K. Pickard, "Inference for discrete Markov fields: the simplest nontrivial case," *J. of the American Statistical Association*, vol. 82, no. 397, pp. 90–96, 1987.

[54] R. W. Conners and C. A. Harlow, "A theoretical comparison of texture algorithms," *IEEE T. Patt. Analy. and Mach. Intell.*, vol. PAMI-2, no. 3, pp. 204–222, 1980.

[55] K. Rose, E. Gurewitz, and G. C. Fox, "Vector quantization by deterministic annealing," *IEEE T. Info. Theory*, vol. 38, pp. 1249–1257, Jul. 1992.

[56] J. E. Lay, *Thermodynamics*. Columbus, Ohio: C. E. Merrill Books, Inc., 1963.